Theoretical calculation and comparison of H diffusion on Cu(111), Ni(111), Pd(111), and Au(111)

Yuta Kataoka [1,*] Jun Haruyama [2] and Osamu Sugino [1,2]

[1]*Department of Physics, Graduate School of Science, The University of Tokyo, Hongo, Bunkyo-ku, Tokyo 113-0033, Japan*

[2]*Institute for Solid State Physics, The University of Tokyo, Kashiwanoha, Kashiwa-shi, Chiba 277-8581, Japan*

(Received 8 December 2022; revised 27 February 2023; accepted 15 May 2023; published 24 May 2023)

We calculated the diffusion coefficient of hydrogen (H) on metal surfaces. In our method, the potential energy surface obtained from the *ab initio* calculations is diagonalized to calculate the wave function of H, which is used to obtain the free energy surface. We combined this free energy surface with transition state theory to obtain the diffusion coefficient. This combination of the free energy surface and transition state theory allowed us to include quantum effects and entropy effects in the transition state theory without stochastic simulations. In addition, by defining diffusion sited from the free energy surface rather than the potential energy surface, the shape and size of the diffusion sites became temperature dependent. The calculated diffusion coefficients were compared with previous studies. Although the present method reproduced the results at and above the crossover temperatures, it was found that more sophisticated quantum mechanical schemes are required at cryogenic temperatures.

DOI: 10.1103/PhysRevB.107.205414

I. INTRODUCTION

Surface diffusion is a topic of fundamental importance not only in catalysis [1] but also in a diverse range of scientific fields such as astrophysics [2] and surface science [3–5]. In contrast to interfacial and bulk diffusion, surface diffusion can be measured directly, and therefore, it is an ideal benchmark system for theoretical analysis [6]. However, our understanding of this phenomenon is incomplete. The quantum effect hampers easy comprehension. In this context, attention has been paid to a hydrogen atom on metal surfaces with a rather flat potential energy surface, where the quantum effect is expected to emerge nontrivially. Interestingly, the strong quantum effect of H [7] changes the diffusion scheme. For example, the zero point energy (ZPE) in the orthogonal direction of the diffusion path creates isotope effect in the diffusion coefficient [8]. Importantly, tunneling is dominant at low temperatures, yielding quantum classical crossover.

The crossover has been measured for several metals [6,9–12], although some results are controversial. For instance, Lauhon and Ho [6] measured the diffusion on a Cu(100) surface using scanning tunneling microscopy and found that crossover occurs at approximately 60 K. Experiments on the Ni(111) surface have also been reported. In early experiments [12,13], crossover was clearly observed with sharp bending in the diffusion coefficient, whereas in a later experiment [14], the curve of the crossover was found to be gradual.

To theoretically interpret the crossover, Nikitin *et al.* [15] applied the transition state wave packet (TSWP) approach [16,17] to Pd(111), where the wave packet was allowed to evolve in imaginary time. The diffusion coefficient was then calculated based on the quantum transition state theory (QTST) proposed by Miller, Schwartz, and Tromp [18]. Moreover, McIntosh *et al.* applied path integral molecular dynamics (PIMD) to Ru(1000) [19]. The diffusion coefficient was then calculated based on the QTST proposed by Voth, Chandler, and Miller [20]. In this method, molecular dynamics simulation of the beads was performed to treat the H atom quantum mechanically, or to consider the incommutable momentum and position operators. Further, Suleimanov [21] applied ring polymer molecular dynamics (RPMD) [22] to Ni(100). Note that the RPMD method is formulated without relying on QTST, unlike the TSWP or PIMD methods. Aside from this technical difference, all these methods stochastically sample the phase space using the Boltzmann weight factor. Therefore, calculations become increasingly demanding as the temperature is reduced and sampling becomes difficult.

In this context, we developed a method that does not rely on a stochastic simulation. We diagonalized the Hamiltonian to obtain the eigenstate. All the states were used to evaluate the Boltzmann factor, and the result was used to calculate the free energy surface (FES). The Boltzmann factor is vanishingly small for a state whose eigenenergy is much smaller than the thermal energy. Therefore, more eigenvalues are required for calculations at higher temperatures than at lower temperatures. In this sense, our method is complementary to conventional ones.

By summing over the eigenstates, the kinetic energy effect is included in the Boltzmann factor, thereby deviating from the conventional classical treatment. In this case, the FES is obtained when summation is performed by restricting the location of an H atom. This fact makes it natural to formulate the transition state theory (TST) based on the FES, although TST has been traditionally formulated based on the potential energy surface (PES). This also modifies the transition state configuration at low temperatures, as discussed below.

In this paper, we theoretically demonstrate our method by applying it to the diffusion of H on the (111) surfaces of Cu, Ni, Pd, and Au. The diffusion coefficient calculated using our

*Corresponding author: y.kataoka@issp.u-tokyo.ac.jp

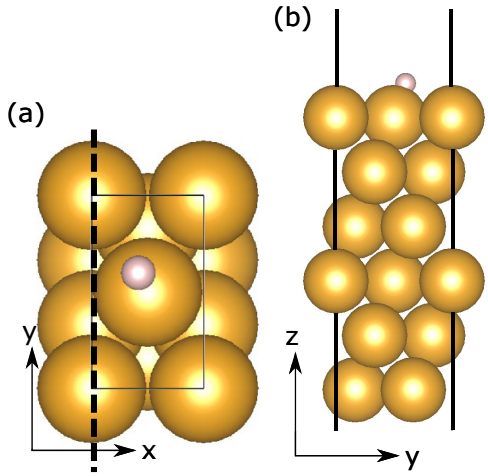

FIG. 1. Six-layer model of H on fcc metal (111) surface. Small (pink) and large (gold) spheres represent H and metal atoms, respectively. (a) Top view and (b) side view.

proposed method is compared with those obtained through experiments and theoretical calculations.

II. METHODS

A. PES calculation

The PES of H on the metal (111) surface was determined by *ab initio* calculations using density functional theory (DFT). The calculations were performed using the electric structure calculation package VASP [23–26]. Throughout the DFT calculations, we used the Perdew-Burke-Ernzerhof (PBE) [27] potential to describe the exchange-correlation of electrons. We also calculated the diffusion coefficient with RPBE [28] but were not significantly different from those calculated with PBE. We also described the Kohn-Sham orbitals using the plane wave within a cutoff energy of 400 eV and the projected augmented wave (PAW) scheme [29]. We optimized the cell parameters of the bulk metal using the Monkhorst-Pack [30] k points ($32 \times 32 \times 32$) and calculated the surface properties from the resulting parameters. A slab model consisting of six layers of the metal with the H atom on the surface was created to determine the PES (Fig. 1). The vacuum for the slab model was approximately 20 Å. The surface was discretized into 12 and 20 points in the x and y directions, respectively, resulting in a total of 240 points. One H atom was placed on a mesh point to relax its position in the z direction. All metal atoms were fixed during the optimization process, which was performed using $8 \times 8 \times 1$ Monkhorst-Pack $k$points with a 400-eV plane wave cutoff. It is worth mentioning here two approximations made in our study. In the first approximation, following the adiabatic approximation of Hopkinson and Robert [31], the metal atoms at the surface are assumed to be stationary on the time scale of fast H dynamics. Suleimanov showed that the motion of metal atoms has a small effect on the diffusion of H in H/Ni(100) [21]. As a second approximation, the PES was approximated as a two-dimensional $V(x, y)$, neglecting the effect of surface corrugations, i.e., the kinetic energy in the direction perpendicular to the surface.

B. FES calculation

The FES was determined based on the PES obtained from the DFT calculations. The FES can also be obtained by performing a molecular dynamics (MD) simulation for each temperature. However, instead of performing an MD simulation, we exploited the periodicity of the system and calculated the wave functions first. Then, we converted these wave functions into the FES. As we fixed all the metal atoms, the PES was expressed using only the positions of the H atom, x and y, as $V(x, y)$. Therefore, the Schrödinger-like equation for H nuclei was expressed as

$$-\frac{\hbar^2}{2m}\nabla^2\phi_i(x,\ y) + V(x,\ y)\phi_i(x,\ y) = \in_i\phi_i(x,\ y), \quad (1)$$

where $\phi_i(x, y)$ and $\in_i$ are the wave function and energy in the ith energy level, respectively. Equation (1) was solved under a periodic condition using a plane wave. In this study, we interpolated the DFT-calculated 12×20 PES into a 48×80 PES using the Fourier series.

The wave function of the H atom nuclei and the energy obtained from Eq. (1) were used to compute the configurational partition function $Q(x, y)$ and FES $F(x, y)$ as follows:

$$Q(x, y) = \frac{\sum_i |\phi_i(x, y)|^2\, e^{-\beta\in_i}}{\sum_j e^{-\beta\in_j}}, \quad (2)$$

$$F(x, y) = -\frac{1}{\beta}[\ln Q(x, y) - \ln Q(x_0, y_0)], \quad (3)$$

where β and (x_0, y_0) are the inverse temperature and reference point, respectively. By calculating FES using Eqs. (1)–(3), we avoided using an MD simulation. There are also methods that do not involve sampling, such as the thermalized microcanonical instanton method [32], and some studies have applied this to one dimensional calculation [33]. In the classical limit, the value of F at the transition state corresponds to the enthalpy required to activate the diffusion plus the entropic contribution in accordance with the original transition state theory. Quantum effect is considered through the discretized energy levels in our formulation. We neglected the excitation of the surface metal atoms, and therefore, the formula is not applicable when the coupling is strong between the diffusing adatom and the surface metal atoms. We also neglected the quantum statistics, or the Fermionic and Bosonic statistics, as conventionally done in the ring polymer simulations.

C. Jump rate and diffusion coefficient

The jump rate was calculated based on the TST developed by Vineyard [34]. In another quantum diffusion method, Kimizuka *et al.* [8] used the same equation but also employed the free energy profile computed based on PIMD. The jump rate from site A to site B and vice versa is expressed as

$$k_{A\to B} = \frac{1}{\sqrt{2\pi m\beta}}\frac{Q_{ts}}{Q_A}, \quad (4)$$

$$k_{B\to A} = \frac{1}{\sqrt{2\pi m\beta}}\frac{Q_{ts}}{Q_B}, \quad (5)$$

where m is the mass of the diffusing particle and the configurational partition function Q is expressed by the integration of

TABLE I. Calculated lattice parameters. The experimental values for the lattice constants are referred from Ref. [36].

Metal	Lattice constant (calculated) (Å)	Lattice constant (experimental) (Å)
Cu	3.64	3.597
Ni	3.51	3.499
Pd	3.94	3.859
Au	4.16	4.065

the FES. For instance,

$$Q_A = \int_A \exp\left[-\beta F(x, y)\right] dxdy \tag{6}$$

transition state. As mentioned before, the entropic and quantum effects are included in Eq. (6).

From the jump rate expressed by Eqs. (4) and (5), the diffusion coefficient was calculated using the random walk model [35]. We first note that D is related to the variance, $\langle \Delta x^2 \rangle$ and $\langle \Delta y^2 \rangle$, by the two-dimensional Einstein relation:

$$4Dt = \langle \Delta x^2 \rangle + \langle \Delta y^2 \rangle, \tag{7}$$

where t is the diffusion interval. The variance is related to the rate by the random walk as follows [35]:

$$\langle \Delta x^2 \rangle = \langle \Delta y^2 \rangle = a^2 \frac{k_{A\to B} k_{B\to A}}{k_{A\to B} + k_{B\to A}} t, \tag{8}$$

where a is the distance between sites A and B. For a, we used the distance between the center of each site. Finally, the diffusion coefficient was expressed as

$$D = \frac{a^2}{2} \frac{k_{A\to B} k_{B\to A}}{k_{A\to B} + k_{B\to A}}. \tag{9}$$

III. RESULTS AND DISCUSSION

A. PES

The lattice constants of the bulk metals were obtained by DFT calculations (Table I). The deviations from experimental values [36] were small, with the largest deviation being that of Au at 2.3%.

The PES was obtained using the lattice constant in Table I (Fig. 2). For all four metal surfaces, the minimum of the PES was located at the fcc site, and the second minimum was located at the hcp site. For Au, the top site was an additional local minimum site. The shape of the Au PES was flatter than the other three metals. Another characteristic of the PES for Au was that the shape of the barrier between the fcc and hcp sites was trapezoidal and flat at the top of the barrier. For the other three metals, the shapes of the barriers between the two sites were parabolic (see Fig. S3 of the Supplemental Material [37].) The energy difference between the hcp and fcc sites was small for Cu and Ni but not for Pd. In other words, the PES for Cu and Ni had almost symmetric hcp and fcc sites, whereas that for Pd had asymmetric hcp and fcc sites. The PES obtained in this calculation was similar to that reported in previous research with a 2 × 2 cell [38].

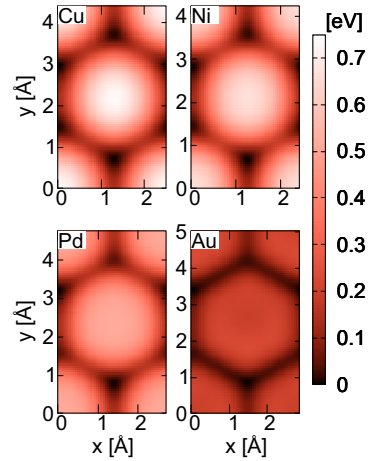

FIG. 2. PES for H on (111) surface of Cu, Ni, Pd and Au. The x and y axes indicate the position of the PES in the x and y directions, respectively. Energy refers to the value at the most stable site, specifically, the fcc site, of each metal. Plot is based on values for a 48 × 80 mesh obtained by Fourier interpolation of results obtained from calculations based on a 12 × 20 mesh.

B. Configurational partition function and FES

The configurational partition function was obtained from Eqs. (1) and (2) by using the calculated PES. The configurational partition function for each temperature is shown in Fig. 3. At a high temperature (1300 K), H was distributed in a wide range of regions. The differences in the H configurational partition function between metal surfaces were small for Cu, Ni, and Pd. For Au, H was distributed in a relatively wider range owing to the flat PES of the Au surface. At a low temperature, the configurational partition function on Au was located along the minimum energy path (MEP) between the hcp and fcc sites, whereas that on Ni and Cu was located around the stable fcc and hcp sites. Pd had a large configurational partition function value at the fcc site owing to the energy related to the asymmetry of the hcp and fcc sites in Pd PES. This can be explained qualitatively as follows. From Eq. (2), especially in the low-temperature region, it was a good approximation to express the configurational partition

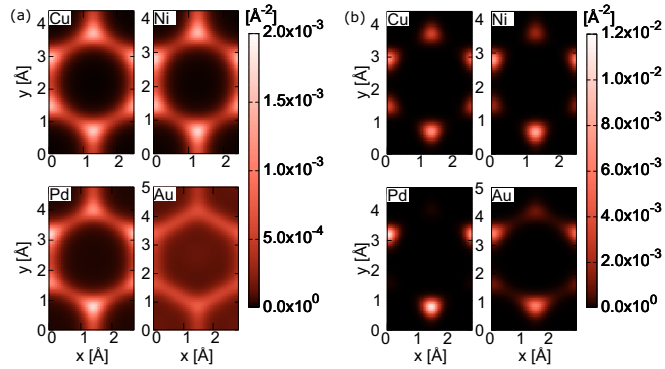

FIG. 3. Configurational partition function of H on the (111) surfaces of Cu, Ni, Pd, and Au. The x and y axes indicate the position of the configurational partition function along the x and y directions, respectively, at (a) 1300 K and (b) 100 K.

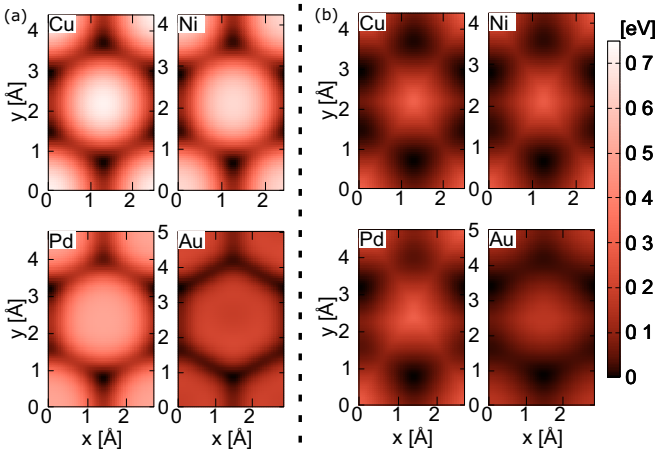

FIG. 4. FES for H on the (111) surface of Cu, Ni, Pd, and Au at (a) 1300 K and (b) 100 K. The x and y axes indicate the position of the FES along the x and y directions, respectively. Energy scale is same as the energy scale of PES (see Fig. 2).

function by using only low energy levels because the contribution from a high energy level will be cut off by the Boltzmann factor. Therefore, the configurational partition function was approximated as

$$Q(x, y) \propto |\phi_{\mathrm{fcc}}(x, y)|^2 + |\phi_{\mathrm{hcp}}(x, y)|^2 \, e^{-\beta \Delta \in}, \qquad (10)$$

where $\Delta \in = \in_{\mathrm{hcp}} - \in_{\mathrm{fcc}}$. From Eq. (10), we see that the large $\Delta \in$ value made the configurational partition function at the hcp sites small (see Fig. SI.2 of the Supplemental Material [37]).

FES was calculated from Eq. (3), and the results are shown in Fig. 4 for 1300 and 100 K. At 1300 K, FES was similar to PES for all metal surfaces. However, FES and PES were never the same because of the ZPE. At 100 K, FES was smaller than that at 1300 K. In classical statistical mechanics, FES is the same as PES. This was because

$$Q(x, y) \propto \exp\left[-\beta V(x, y)\right], \qquad (11)$$

$$F(x, y) = V(x, y) - V(x_0, y_0), \qquad (12)$$

where Eq. (12) is obtained by substituting Eq. (13) into Eq. (3). Therefore, the temperature dependence of FES comes from quantum effects. FES at 1300 and 100 K were similar for Au, however, for Cu, Ni, and Pd, the fcc and hcp regions were expanded at 100 K. This indicates that the quantum effects of H on Cu, Ni, and Pd were stronger than that of H on Au. These facts characterize the diffusion coefficients (Fig. 7) and crossover temperature (Table II).

C. Jump rate and diffusion coefficients

We calculated the jump rate and diffusion coefficients between the fcc and hcp sites. To calculate the jump rate, we calculated Q_{fcc}, Q_{hcp}, and Q_{ts}. For integration in Eq. (6), the integral region for the fcc and hcp sites and the transition state had to be defined. In this study, we defined the fcc and hcp sites as shown in Fig. 5. The transition state was drawn by connecting the saddle point with the ridgeline (black line in Fig. 5), and the blue and orange region surrounded by the transition state were defined as the hcp and fcc sites, respectively.

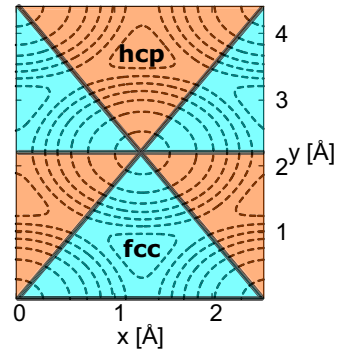

FIG. 5. Regions of the hcp (orange) and fcc (blue) sites. The x and y axes indicate the position of PES along the x and y directions, respectively. The contour indicates the PES of H on Cu (see Fig. 2). The black line between the two sites indicates the transition state. Q_{fcc}, Q_{hcp}, and Q_{ts} are calculated by integrating $Q(x, y)$ in the blue area, orange area, and black line, respectively.

The jump rates were calculated from Eqs. (4) and (5), and the results are shown in Fig. 6. As the temperature decreases, the jump rate changed from its classical value. For the jump rate from the fcc to the hcp site, the temperature dependence on the jump rate vanished and turned into a straight line. By contrast, we found that the jump rate for Pd tended to increase after the crossover. In Sec. III B, we discussed the configurational partition function at low temperatures using Eq. (10). As the hcp configurational partition function decreases with decreasing temperature, the jump rate becomes artificially high. This can be confirmed from Eq. (4). As mentioned earlier, the asymmetry was the largest for Pd, and this led to the formation of a large curve in the jump rate. However, this increase at low temperature may not have a physical meaning because the QTST used in this study is known to break down at temperatures lower than that at the crossover [39].

From the jump rate, we calculated the diffusion coefficient (Fig. 7). The dotted straight line indicates the diffusion coefficient for the classical case. The curve was found for all H diffusion coefficients of the metal surfaces. Compared to the other three metal surfaces, Au had a lower crossover temperature T_{c}. This was attributable to the shape of the PES. As mentioned in Sec. III A, the barrier between hcp and fcc has a trapezoidal shape, and this affects the tunneling regime. This was also found in the one-dimensional model calculation [33]. In Ref. [33], owing to the shape of the potential for the Au surface, T_{c} is calculated from Eq. (13):

$$T_{\mathrm{c}} = \frac{\hbar}{k_B} \frac{E_a}{2 \int \sqrt{2mV(y)}dy}, \qquad (13)$$

where E_a and $V(y)$ are the activation energy and potential along the MEP (the one-dimensional potential is shown in the Supplemental Material [37]), respectively. The calculated T_{c} is shown in Table II. T_{c} was located at the curvature of the diffusion coefficient. From the PES, the diffusion coefficient on the Au surface may have been the largest because the barrier was the smallest for Au. However, the order of the diffusion coefficient changed with Cu and Ni at around 80 K. Among

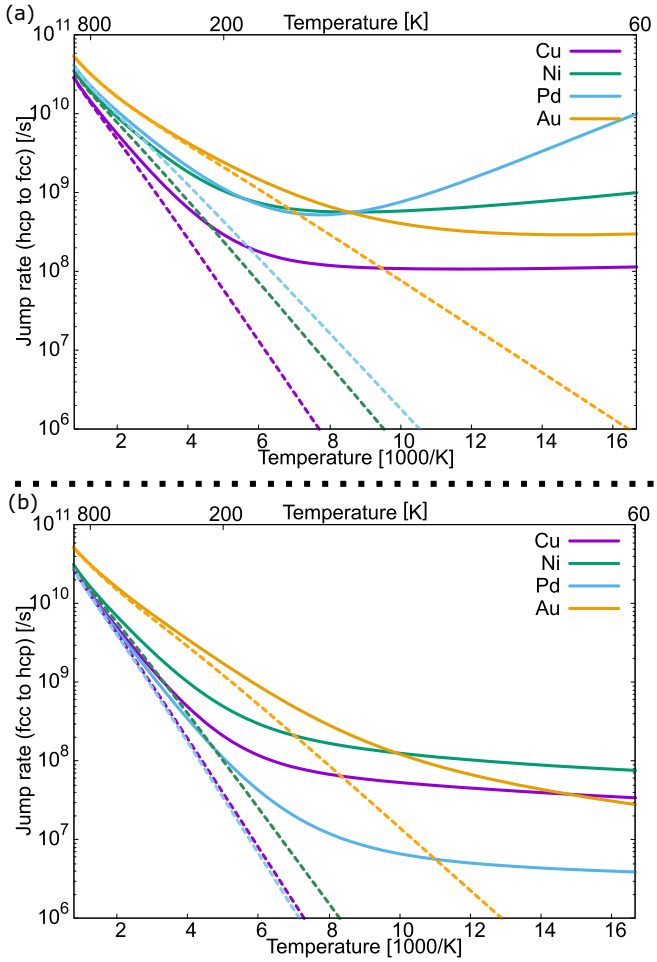

FIG. 6. Jump rate of H on (111) surfaces of Cu, Ni, Pd, and Au. Jump rates from the (a) hcp to fcc site and (b) fcc to hcp site. The bottom and top x axes indicate the inverse temperature and temperature, respectively. The y axis indicates the diffusion coefficient. The classical results are indicated by dotted lines.

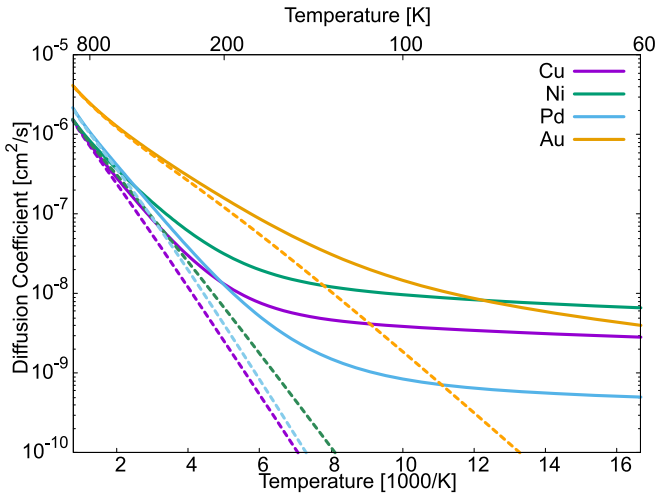

FIG. 7. Diffusion coefficient for H on the (111) surface of Cu, Ni, Pd, and Au. The bottom and top x axes indicate the inverse temperature and temperature, respectively. The y axis indicates the diffusion coefficient. The classical results are indicated by dotted lines.

TABLE II. Calculated crossover temperature.

Metal	K
Cu	93.9
Ni	90.6
Pd	80.1
Au	52.4

the four metal surfaces used in this study, Pd had the smallest diffusion coefficient value, and this may be attributable to the asymmetric shape of the PES for Pd. When we imagine the double well potential, we believe that tunneling is likely to occur with the same energy level. To conform with the results for Pd, we used the one-dimensional model potential that can change the height of the two wells. We used an asymmetric function:

$$V(x) = \begin{cases} \frac{1}{2}\omega^2\left(x^4 - \frac{3x^2}{2} - x\cos\phi\right) & \text{when } -\frac{\sqrt{5}}{2} < x < \frac{\sqrt{5}}{2} \\ \frac{1}{2}\omega^2\left(x^2 - x\cos\phi - \frac{25}{16}\right) & \text{otherwise.} \end{cases}, \tag{14}$$

where ω is the strength of the potential, and ϕ is the degree of asymmetry at which the potential is symmetric for $\phi = \pi/2$ and asymmetric otherwise. The potential exhibits two minima when $0 < \phi < \pi$ [Fig. 8(a)]. The Hamiltonian is expressed as

$$H = -\frac{1}{2}\frac{d^2}{dx^2} + V(x). \tag{15}$$

We obtained the diffusion coefficients by using Eq. (15) and Eqs. (1)–(9). The results are plotted in Fig. 8(b) as a function of the barrier heights corresponding to the left and right minima, that is, the difference in the energy of the potential in the transition state and at the local minimum. The diffusion coefficient was the largest in the symmetric case, as can be observed by moving horizontally or vertically [Fig. 10(b)]. Thus, the symmetric PES gave the largest diffusion coefficient.

D. Comparison with other works

We compared the diffusion coefficients calculated using our methods and the TSWP [15] (Fig. 9). Our calculated diffusion coefficients were smaller than those calculated by TSWP in both the classical and quantum cases. This difference is due to the difference in the TSTs used. The difference in the quantum diffusion coefficients becomes smaller as the temperature gets lower, and the qualitative behavior reproduces the calculations of previous studies.

We compared our result of H diffusion on Ni(111) with experiments [12–14] and theoretical calculation [31] (Fig. 10). Our calculated diffusion coefficients were smaller than those calculated by TSWP in both the classical and quantum cases. Although there was the difference in value, the crossover occurs similarly as the temperature is decreased. Our results overestimate the experiments although the crossover behavior is reproduced reasonably well. The reason for the discrepancy is not clear, but one might rule out the possibility that the electronic friction will play a role because of the low velocity that the diffusing H atom can take thermally. Also, our results confirm isotope effects, which are not confirmed

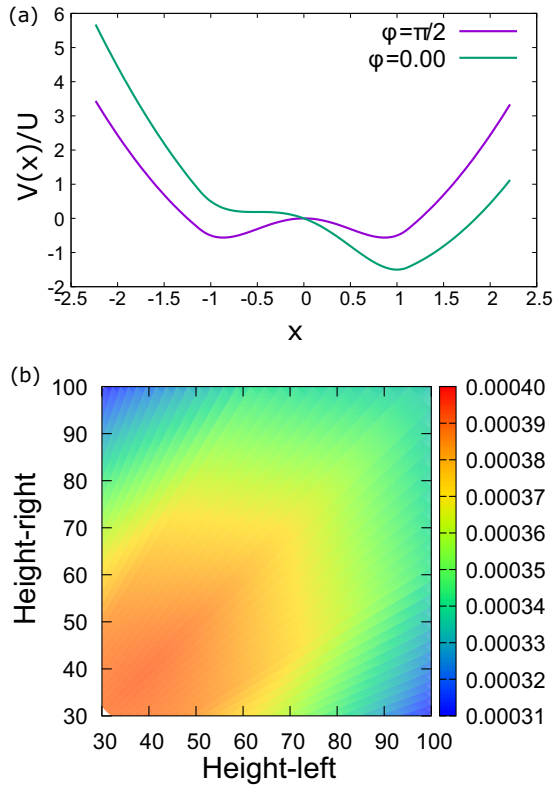

FIG. 8. (a) Plot of $V(x)$ at different asymmetry parameters ϕ. Potential is scaled by $U = \frac{1}{2}\omega^2$. $V(x)$ is symmetric for $\phi = \pi/2$ and asymmetric otherwise. (b) Diffusion coefficient D at 100 K plotted against parameters. For ease of understanding, D is plotted against the height of the potential in the transition state, $V(x_{\rm tst})$, seen from the left-hand side of the local minimum, or "height-left," and the height seen from the right-hand side, or "height-right."

by experimental results. Note that prior PACMD calculations significantly overestimated the experiment. The TST we used in this calculation is semiclassical, and the time dependent transmission coefficient [40], which is included in TSWP and RPMD but not in PIMD, is neglected. However, this factor is

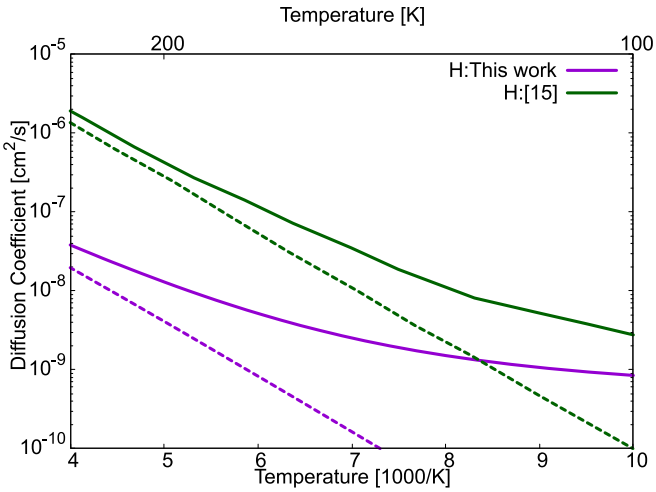

FIG. 9. Diffusion coefficient of H on the Pd(111) surface. The purple line indicates our result, and the green line indicates that calculated by TSWP [15]. Dotted lines indicate the classical case.

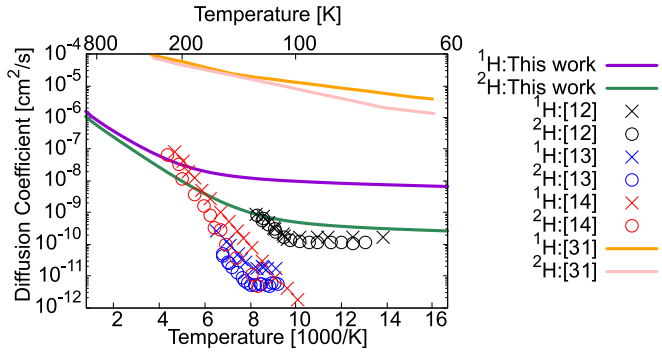

FIG. 10. Diffusion coefficient of H on Ni(111) surface. Purple and green lines show the results obtained for ^{1}H and ^{2}H, respectively, using our methods. The black crosses and circles indicate the results of ^{1}H and ^{2}H, respectively, from previously published experiments [12]. The blue crosses and circles indicate the results of ^{1}H and ^{2}H, respectively, from previously published experiments [13]. The red crosses and circles indicate the results of ^{1}H and ^{2}H, respectively, from previously published experiments [14]. The red orange and pink lines indicate the results of ^{1}H and ^{2}H, respectively, from previously published calculation [31].

important at temperatures lower than T_c. Therefore, it is still questionable whether this theoretical calculation can reproduce the experiment quantitatively at very low temperature.

IV. FURTHER DISCUSSION

To obtain the diffusion coefficient for H, we defined the regions of the hcp and fcc sites as shown in Fig. 5. However, we can define the regions in a different way. Figure 5 was defined based on the PES; however, we can alternatively define sites based on the FES. The FES changed its shape with a change in temperature. This means that if we define the sites using FES, the regions of hcp and fcc sites change between temperatures. By this definition, a position at which the slope of the FES was zero defined the sites. An example of the site definition is shown in Fig. 11. Compared to the site definition

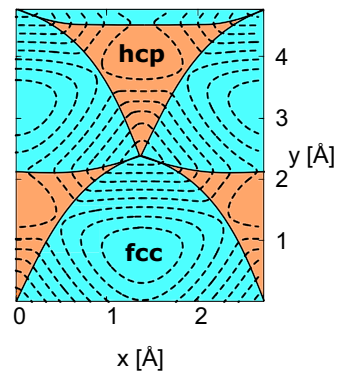

FIG. 11. Regions of hcp (orange) and fcc (blue) sites. The x and y axes indicate the position of FES for the x and y directions, respectively. The contour indicates the FES of H on Pd at 60 K. The black line between two sites indicates the transition state. $Q_{\rm fcc}$, $Q_{\rm hcp}$, and $Q_{\rm ts}$ are calculated by integrating $Q(x, y)$ in the blue area, orange area, and along black line, respectively.

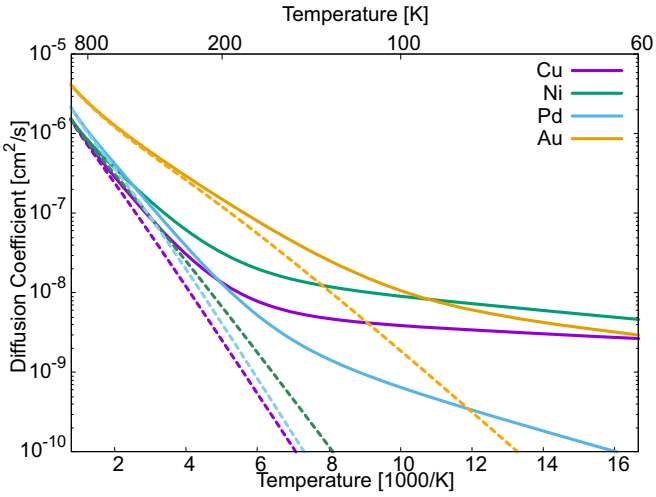

FIG. 12. Diffusion coefficient for H on the (111) surface of Cu, Ni, Pd, and Au as calculated from the site defined by FES. The bottom and top x axes indicate the inverse temperature and temperature, respectively. The y axis indicates the diffusion coefficient. The classical result is indicated by the dotted lines.

based on PES, the size and shape of the hcp and fcc sites were not symmetric.

The diffusion coefficient was then calculated, and the result is shown in Fig. 12. At high temperatures, the diffusion coefficient was the same as that obtained based on the PES defined site. However, the FES-based diffusion coefficient differs from the PES-based one at low temperatures. This can be explained by comparing our calculation methods with RPMD-based methods. In our calculation, the time dependent transmission coefficient was considered to be equal to 1 [20]. At high temperatures, the time dependent transmission coefficient is approximately 1, however at temperatures below T_c, it is smaller than 1 [21]. For the RPMD calculation, this factor makes the diffusion coefficient independent of the transition state definition. However, in our method, this factor was not included, and it causes a dependence on the regional definition and breakdown at low temperatures [39].

V. CONCLUSION

We proposed a calculation method of FES that does not require sampling. In this method, we use the basis set of the Hamiltonian instead of the position and momentum used in PIMD. Our method is effective for small surfaces with periodic conditions because we can diagonalize the Hamiltonian of the system easily. Moreover, at low temperature, the contribution from high energy to FES is cut out by the Boltzmann factor, and this reduces the calculation cost. By using this method, we calculated the diffusion coefficient of H on four (111) metal surfaces: Cu, Ni, Pd, and Au. Cu and Ni have approximately symmetric energy levels on their hcp and fcc sites, but Pd and Au do not. This symmetry makes the diffusion coefficient bigger for Cu and Ni. Au has a flat PES shape between the fcc and hcp sites; this lowers the crossover temperature.

By using the proposed method, we calculated the diffusion coefficient without any sampling, thereby reducing our calculation cost. However, as the degrees of freedom increase, the calculation cost increases. This makes it difficult to calculate, for instance, the diffusion coefficient on a moving surface. We can include these effects in RPMD [21]. Additionally, at very low temperatures ($T < T_c$), the TST we used in our method breaks down [39] because of our semiclassical approach. We will calculate the time dependent transmission coefficient in our future studies.

ACKNOWLEDGMENTS

We thank Dr. T. Kawatsu for the fruitful discussions. This work was supported by the Ministry of Education, Culture, Sports, Science and Technology (MEXT), Japan, through the "Program for Promoting Research on the Supercomputer Fugaku" (Fugaku Battery & Fuel Cell Project, Grant No. JPMXP1020200301) and the Japan Society for the Promotion of Science (JSPS) through a Grant-in-Aid for Scientific Research on Innovative Areas ("Hydrogenomics," Grant No. 18H05519). Most of the computations were performed on supercomputers at the Supercomputing Division, Information Technology Center, The University of Tokyo, and the Institute for Solid State Physics, The University of Tokyo.

[1] N. Lopez, Z. Łodziana, F. Illas, and M. Salmeron, When Langmuir Is Too Simple: H_2 Dissociation on Pd(111) at High Coverage, Phys. Rev. Lett. **93**, 146103 (2004).

[2] T. P. M. Goumans and J. Kästner, Hydrogen-atom tunneling could contribute to H2 formation in space, Angew. Chem. Int. Ed. **49**, 7350 (2010).

[3] J. V. Barth, Transport of adsorbates at metal surfaces: from thermal migration to hot precursors, Surf. Sci. Rep. **40**, 75 (2000).

[4] G. Antczak and G. Ehrlich, The beginnings of surface diffusion studies, Surf. Sci. **589**, 52 (2005).

[5] J. D. Doll and A. F. Voter, Recent developments in the theory of surface diffusion, Annu. Rev. Phys. Chem. **38**, 413 (1987).

[6] L. J. Lauhon and W. Ho, Direct Observation of the Quantum Tunneling of Single Hydrogen Atoms with a Scanning Tunneling Microscope, Phys. Rev. Lett. **85**, 4566 (2000).

[7] T. E. Markland, S. Habershon, and D. E. Manolopoulos, Quantum diffusion of hydrogen and muonium atoms in liquid water and hexagonal ice, J. Chem. Phys. **128**, 194506 (2008).

[8] H. Kimizuka, S. Ogata, and M. Shiga, Unraveling anomalous isotope effect on hydrogen diffusivities in Fcc metals from first principles including nuclear quantum effects, Phys. Rev. B **100**, 024104 (2019).

[9] R. DiFoggio and R. Gomer, Diffusion of hydrogen and deuterium on the (110) plane of tungsten, Phys. Rev. B **25**, 3490 (1982).

[10] C. Dharmadhikari and R. Gomer, Diffusion of hydrogen and deuterium on the (111) Plane of tungsten, Surf. Sci. **143**, 223 (1984).

[11] S. M. George, A. M. DeSantolo, and R. B. Hall, Surface diffusion of hydrogen on Ni(100) studied using laser-induced thermal desorption, Surf. Sci. **159**, L425 (1985).
[12] T. S. Lin and R. Gomer, Diffusion of ^{1}H and ^{2}H on the Ni(111) and (100) planes, Surf. Sci. **255**, 41 (1991).
[13] A. Lee, X. D. Zhu, A. Wong, L. Deng, and U. Linke, Observation of diffusion of H and D on Ni(111) from over-barrier hopping to nonactivated tunneling, Phys. Rev. B **48**, 11256 (1993).
[14] G. X. Cao, E. Nabighian, and X. D. Zhu, Diffusion of Hydrogen on Ni(111) over a Wide Range of Temperature: Exploring Quantum Diffusion on Metals, Phys. Rev. Lett. **79**, 3696 (1997).
[15] I. Nikitin, W. Dong, H. F. Busnengo, and A. Salin, Diffusion of a hydrogen atom on the Pd(1 1 1) surface: Quantum transition state wave packet approach, Surf. Sci. **547**, 149 (2003).
[16] J. C. Light and D. H. Zhang, The quantum transition state wavepacket method, Faraday Discuss. **110**, 105 (1998).
[17] D. H. Zhang, J. C. Light, and S. Y. Lee, Transition state wave packet study of hydrogen diffusion on Cu(100) surface, J. Chem. Phys. **111**, 5741 (1999).
[18] W. H. Miller, S. D. Schwartz, and J. W. Tromp, Quantum mechanical rate constants for bimolecular reactions, J. Chem. Phys. **79**, 4889 (1983).
[19] E. M. McIntosh, K. Thor Wikfeldt, J. Ellis, A. Michaelides, and W. Allison, Quantum effects in the diffusion of hydrogen on Ru(0001), J. Phys. Chem. Lett. **4**, 1565 (2013).
[20] G. A. Voth, D. Chandler, and W. H. Miller, Rigorous formulation of quantum transition state theory and its dynamical corrections, J. Chem. Phys. **91**, 7749 (1998).
[21] Y. V. Suleimanov, Surface diffusion of hydrogen on Ni(100) from ring polymer molecular dynamics, J. Phys. Chem. C **116**, 11141 (2012).
[22] I. R. Craig and D. E. Manolopoulos, Quantum statistics and classical mechanics: Real time correlation functions from ring polymer molecular dynamics, J. Chem. Phys. **121**, 3368 (2004).
[23] G. Kresse and J. Hafner, Ab initio molecular dynamics for liquid metals, Phys. Rev. B **47**, 558 (1993).
[24] G. Kresse and J. Furthmüller, Efficient iterative schemes for ab initio total-energy calculations using a plane-wave basis set, Phys. Rev. B. **54**, 11169 (1996).
[25] G. Kresse and D. Joubert, From ultrasoft pseudopotentials to the projector augmented-wave method, Phys. Rev. B **59**, 1758 (1999).
[26] G. Kresse and J. Furthmüller, Efficiency of ab-initio total energy calculations for metals and semiconductors using a plane-wave basis set, Comput. Mater. Sci. **6**, 15 (1996).
[27] J. P. Perdew, K. Burke, and M. Ernzerhof, Generalized Gradient Approximation Made Simple, Phys. Rev. Lett. **77**, 3865 (1996).
[28] B. Hammer, L. B. Hansen, and J. K. Nørskov, Improved adsorption energetics within density-functional theory using revised Perdew-Burke-Ernzerhof functionals, Phys. Rev. B **59**, 7413 (1999).
[29] P. E. Blöchl, Projector augmented-wave method, Phys. Rev. B **50**, 17953 (1994).
[30] H. J. Monkhorst and J. D. Pack, Special points for brillouin-zone integrations, Phys. Rev. B **13**, 5188 (1976).
[31] A. R. Hopkinson and M. I. J. Probert, Quantum diffusion of H/D on Ni(111)—a partially adiabatic centroid MD study, J. Chem. Phys. **148**, 102339 (2018).
[32] J. O. Richardson, Microcanonical and thermal instanton rate theory for chemical reactions at all temperatures, Faraday Discuss. **195**, 49 (2017).
[33] W. Fang, J. O. Richardson, J. Chen, X.-Z. Z. Li, and A. Michaelides, Simultaneous Deep Tunneling and Classical Hopping for Hydrogen Diffusion on Metals, Phys. Rev. Lett. **119**, 126001 (2017).
[34] G. H. Vineyard, Frequency factors and isotope effects in solid state rate processes, J. Phys. Chem. Solids **3**, 121 (1957).
[35] J. D. Wrigley, M. E. Twigg, and G. Ehrlich, Lattice walks by long jumps, J. Chem. Phys. **93**, 2885 (1990).
[36] W. P. Davey, Precision measurements of the lattice constants of twelve common metals, Phys. Rev. **25**, 753 (1925).
[37] See Supplemental Material at http://link.aps.org/supplemental/10.1103/PhysRevB.107.205414 for the details of two dimensional calculation and the diffusion coefficient for one dimensional calculation. The Supplemental Material also contains Ref. [15].
[38] L. Kristinsdóttir and E. Skúlason, A systematic DFT study of hydrogen diffusion on transition metal surfaces, Surf. Sci. **606**, 1400 (2012).
[39] J. O. Richardson and S. C. Althorpe, Ring-polymer molecular dynamics rate-theory in the deep-tunneling regime: Connection with semiclassical instanton theory, J. Chem. Phys. **131**, 214106 (2009).
[40] R. Collepardo-Guevara, I. R. Craig, and D. E. Manolopoulos, Proton transfer in a polar solvent from ring polymer reaction rate theory, J. Chem. Phys. **128**, 144502 (2008).